**RAA 2021** Vol. **21** No. **8**, 202(12pp) doi: 10.1088/1674-4527/21/8/202

*http://www.raa-journal.org* *http://iopscience.iop.org/raa*

*Research in Astronomy and Astrophysics*

# LASPM: the LAMOST stellar parameter pipeline for M-type stars and application to the sixth and seventh data release (DR6 and DR7)

Bing Du (杜冰)[1], A-Li Luo (罗阿理)[1,2⋆], Shuo Zhang (张硕)[3], Xiao Kong (孔啸)[1], Yan-Xin Guo (郭炎鑫)[1], Yin-Bi Li (李荫碧)[1,2], Fang Zuo (左芳)[1,2], You-Fen Wang (王有芬)[1], Jian-Jun Chen (陈建军)[1] and Yong-Heng Zhao (赵永恒)[1,2]

[1] CAS Key Laboratory of Optical Astronomy, National Astronomical Observatories, Beijing 100101, China; *lal@nao.cas.cn*

[2] University of Chinese Academy of Sciences, Beijing 100049, China

[3] Department of Astronomy, School of Physics, Peking University, Beijing 100871, China

Received 2021 February 2; accepted 2021 April 10

**Abstract** The molecular-rich atmospheres of M type stars complicate our understanding to their atmospheric properties. Recently, great progress has been made in atmospheric modeling of M-type stars, and we take advantage of the updated BT-Settl model grid to develop a pipeline LASPM to measure atmospheric parameters ($T_{\rm eff}$, log $g$, [M/H]) of M-type stars from low-resolution spectra. The pipeline was applied to the sixth and seventh data release (DR6 & DR7) of Large Sky Area Multi-Object Fiber Spectroscopic Telescope (LAMOST), which released atmospheric parameters for 610 419 and 680 185 M-type spectra, respectively. The key algorithm is to find the best-matching for templates in the synthetic spectral library for an observed spectrum, and then minimizing $\chi^2$ through a linear combination of five best-matching templates. The intrinsic precisions of the parameters were estimated by using the multiple epoch observations for the same stars, which are 118 K, 0.20 dex, 0.29 dex for $T_{\rm eff}$, log $g$, and [M/H] respectively. The $T_{\rm eff}$ and log $g$ are consistent with the spectral and luminosity classifications by LAMOST 1D pipeline, and the loci of giants and dwarfs both on spectral index and color-magnitude diagrams show the validity. The metallicities of LASPM are also checked with the selected members of four open clusters (NGC 2632, Melotte 22, ASCC_16, and ASCC_19), which are consistent without any bias. Comparing the results between LASPM and the APOGEE Stellar Parameter and Chemical Abundance Pipeline (ASPCAP), there is a scatter of 73 K, 0.22 dex, 0.21 dex for $T_{\rm eff}$, log $g$, and [M/H], respectively.

**Key words:** atmospheric parameters — data analysis— spectrographs

## 1 INTRODUCTION

The stellar parameters of M-type stars is important for the study of the Milky Way, while determining atmospheric parameters for low-mass stars is a long-standing problem in astronomy because of the complex, molecular-rich atmospheres. Previously, each stellar parameter of low-mass stars was generally separately dealt with. For example, Ségransan et al. (2003) determined the angular diameter of four very low-mass stars using interferometry, and then derived masses and surface gravities with the mass-luminosity relations. Rojas-Ayala et al. (2012) calculated the effective temperatures for 133 M dwarfs by investigating the near-infrared $K$-band spectra. Boyajian et al. (2012) estimated the effective temperatures for nearby K and M dwarfs through bolometric fluxes from photometry and interferometrically determined radii.

Fundamental stellar parameters of low-mass stars such as effective temperature ($T_{\rm eff}$), surface gravity (log $g$), and metallicity ([M/H]) are model dependent to some extent. Lacking of reliable models, the large-scale spectroscopic surveys, for example, the Sloan Digital Sky Survey (SDSS; York et al. 2000) and the Large Sky Area Multi-Object Fiber Spectroscopic Telescope (LAMOST; Cui et al. 2012; Deng et al. 2012) did not provide parameters for M-type stars. Fortunately, the atmosphere modeling of low-mass stars has been developed with the parallel improvement of computing capacities in the recent decade, such as the PHOENIX BT-Settl model , which incorporates the revised

⋆ Corresponding author

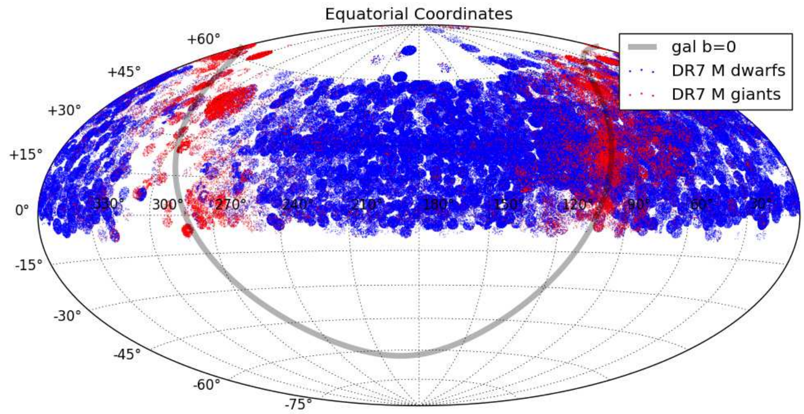


**Fig. 1** The sky distribution of the 'footprints' of the selected 570 228 M stars from LAMOST-DR7 with *red* for giants and *blue* for dwarfs. The projection is in Equatorial Coordinates.

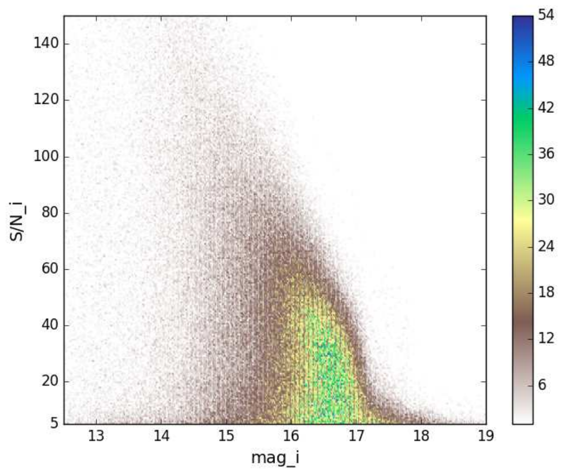


**Fig. 2** The number of stars in the $i$ band S/N – magnitude plane. The different colors are for levels of different star number values.

solar abundances along with updated atomic and molecular line opacities (Allard et al. 2012, 2013). Recently, Rajpurohit et al. (2016, 2018) and Passegger et al. (2016) used the updated BT-Settl model and PHOENIX-ACE model respectively to estimate the fundamental stellar parameters $T_{\rm eff}$, log $g$ and [M/H] of the M dwarfs. These parameter measurements of M-type stars are obtained from a few to a few dozen high-resolution spectra, and some efforts also have been made for low-resolution spectra using the updated BT-Settl model, for example, Rajpurohit et al. (2013) determined $T_{\rm eff}$ of bright M dwarfs from the low-resolution optical spectra and concluded that the updated BT-Settl synthetic spectra reproduce the slope of the observed spectra very well. Based on the experience of the above experts, we took advantage of the updated BT-Settl model grids to develop the LASPM pipeline, and

**Table 1** Parameter Space of the Grid Used in This Work

| | Range | Step size |
|---|---|---|
| $T_{\rm eff}$ (K) | 2300 – 4300 | 100 |
| log $g$ (dex) | 0 – 6.0 | 0.5 |
| [M/H] (dex) | –2.5 – +0.5 | 0.5 |
| $[\alpha/{\rm M}]$(dex) | 0 – +0.4 | 0.2 |

applied to the LAMOST low resolution M-type spectra (R $\sim$ 1800). The measurement of parameters for M-type stars extends the capability of the LAMOST stellar parameter pipeline (LASP) deal with cool stars.

The LAMOST DR7 has collected more than 10 million low-resolution spectra, including more than 700 000 M-type spectra. We measured parameters for 680 185 M-type spectra and integrated them into the M star catalog of LAMOST DR7, in which 610 419 has been released in DR6. The number far exceeds the entries of the previous largest M-type stellar parameter catalog (including more than 70 000 M-type stars), which were obtained from the Apache Point Observatory Galactic Evolution Experiment (APOGEE) of the SDSS Data Release 16 (DR16; Jönsson et al. 2020).

This paper provides a thorough description of LASPM pipeline and presents the results of its performance. This paper is organized as follows. In Section 2, we describe the BT-Settl model used in this work. In Section 3, we briefly describe the LAMOST observations and data reduction, and details the pipeline and methods for the determination of stellar parameters in M-type stars. Section 4 presents the results and comparisons with ASPCAP spectroscopic stellar parameters. Finally, the summary and discussion are presented in Section 5.

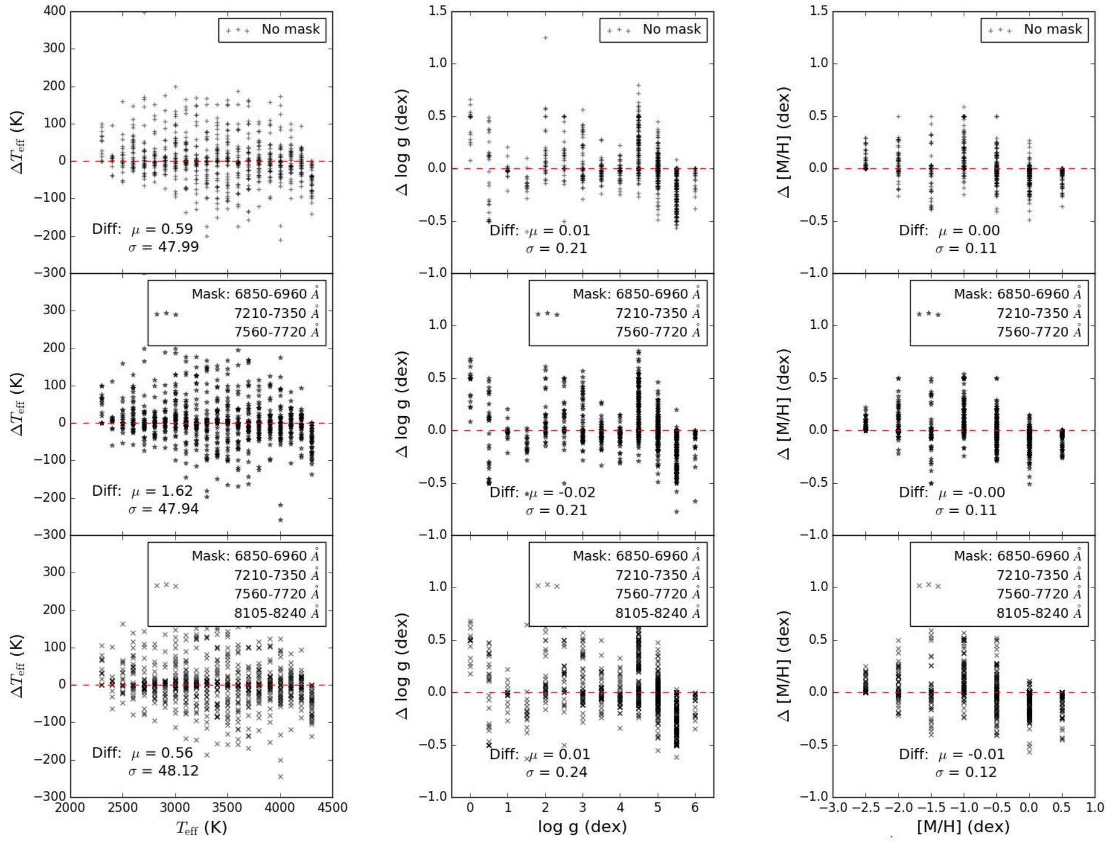


**Fig. 3** The differences between actual parameters and the derived parameters of different masks. From Left to right columns: the differences of $T_{\rm eff}$, log $g$, and [M/H]. From top to bottom panels: no mask, mask (6850–6960Å , 7210–7350Å, 7560–7720 Å), and mask (6850–6960Å, 7210–7350Å, 7560–7720Å, 8105–8240 Å).

## 2 PHOENIX BT-SETTL MODEL GRIDS

In the pipeline, the model version of BT-Settl is CIFIST2011 (Allard et al. 2011, 2012), which were updated in 2013, and synthetic spectra were calculated with the radiative transfer code named "PHOENIX" (Allard et al. 2001). The version of CIFIST2011 includes the dust formation and gravitational settling, making decisive progress in different aspects, including the treatment of convection, updated molecular line lists and better solar abundance (Allard et al. 2012). The updated line list of water vapor was taken from Barber et al. (2006), in which the IR region of synthetic spectra has been improved especially for M-type stars. The CaH, VO and TiO line lists were taken from Plez (1998), MgH from Skory et al. (2003) and Weck et al. (2003), FeH and CrH from Dulick et al. (2003) and Chowdhury et al. (2006), and NH3 from Yurchenko et al. (2011). The alpha elements are from Caffau et al. (2009) and Caffau et al. (2011), including both enhanced and the solar abundance.

The coverage of $T_{\rm eff}$, log $g$, and [M/H] in the BT-Settl CIFIST2011 grid are 300 to 8000 K, 0.0 to 6.0 dex, and –2.5 to +0.5 dex with steps of 100 K, 0.5 dex, and 0.5 dex, respectively. For Alpha-enhancement, [$\alpha$/H] = 0.4 when [M/H] $\leq$ –1.0, [$\alpha$/H] = 0.2 when [M/H] = –0.5, and no alpha-enhancement when [M/H] $\geq$ 0.0. We only adopted a part of the grid covering the parameter space of M-type stars, which is shown in Table 1.

## 3 THE PARAMETER DETERMINATION METHODS OF LASPM

We designed the LASPM based on the PHOENIX BT-Settl Model Grids. The pipeline employed a series of procedures including spectral region selection, pre-processing, $\chi^2$matching, and linear combination, etc. The methods used in this work are detailed in the following, and we will introduce the LAMOST observation and data reduction for M type stars in the beginning.

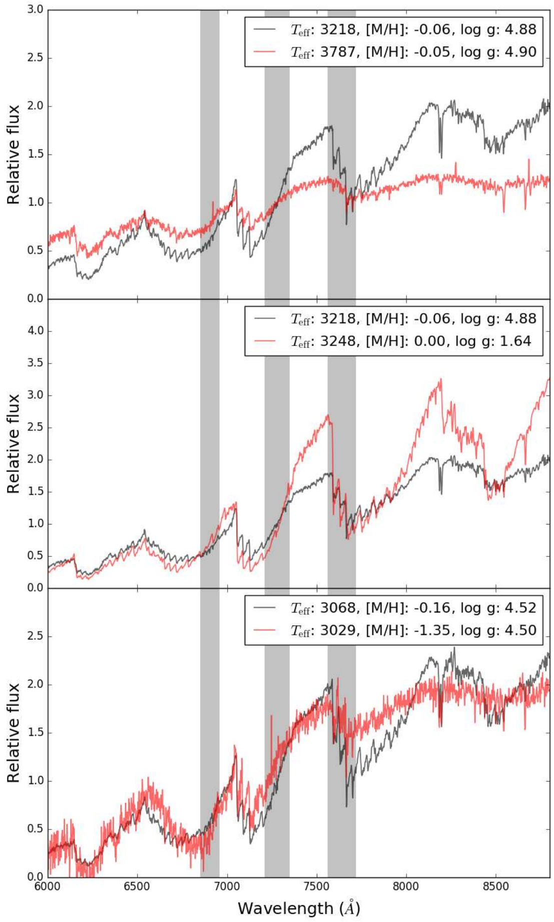


**Fig. 4** The spectral regions used to determine $T_{\rm eff}$, [M/H], and log $g$ for five stars. Spectral comparisons of different temperatures (*top*), of different surface gravities (*middle*), and of different metallicities (*bottom*). The *gray filled areas* are the masked bands to exclude the Earth's atmosphere lines.

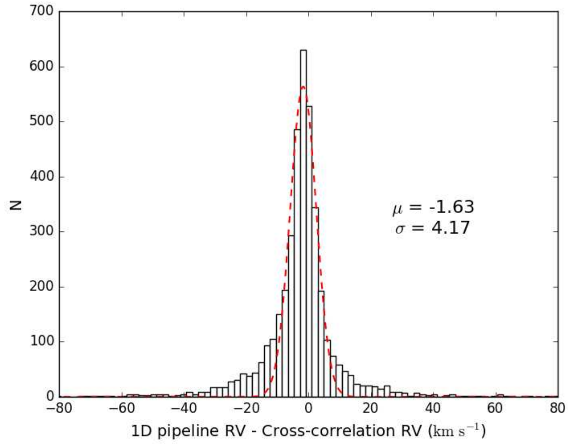


**Fig. 5** Histograms of differences between the 1D pipeline RVs and the RVs estimated using the cross-correlation method.

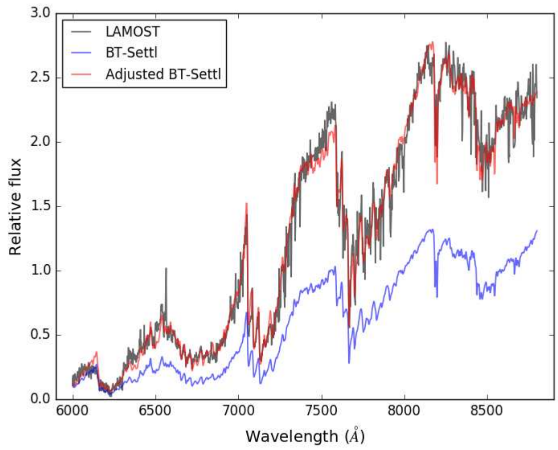


**Fig. 6** One example of the LAMOST observed spectrum (*black*), the BT-Settl spectrum (*blue*), and the adjusted BT-Settl spectrum (*red*).

### 3.1 Observations and Data Reduction

LAMOST DR7 includes more than 10 million low-resolution spectra (R $\sim$ 1800), covering the wavelength range from 3800 – 9000 Å. The raw data were reduced by the LAMOST 2D pipeline (Luo et al. 2015), including bias subtraction, correction of flat field, extraction of spectra, wavelength calibration, sky subtraction, and flux calibration. The extracted spectra were analyzed by the LAMOST 1D pipeline (Luo et al. 2015) to recognize the spectral classes, as well as to determine the radial velocity (RV) for stars.

Totally, the LAMOST 1D pipeline recognized 707 614 M-type spectra, and classified them to spectral types of M1 – M9 and roughly luminosity classes of M giant (gM) and M dwarfs (dM). Considering that the features of M stars are dominant in the $i$-band, we excluded the spectra with $i$-band Signal-to-Noise ratio (S/N) less than 5.0. Finally, we analyzed 687 916 M-type spectra (570 228 stars) in DR7 to try to determine their stellar parameters. The sky distribution of the 'footprints' of the 570 228 stars was shown in Figure 1, and the contour plot of their number in the $i$ band S/N – magnitude plane is shown in Figure 2. We noted that our sample consisted mainly of stars with $i$ band magnitudes ranging from 16–17.

### 3.2 Spectral Region Selection

It is important to chose spectral regions including the obvious M-type spectral features that are sensitive to all stellar parameters $T_{\rm eff}$, log $g$ and metallicity. Most of the features in M-type spectra are dominant in the red part of LAMOST spectra, and the S/N of the red part of an M-type spectrum is generally higher than that of the blue

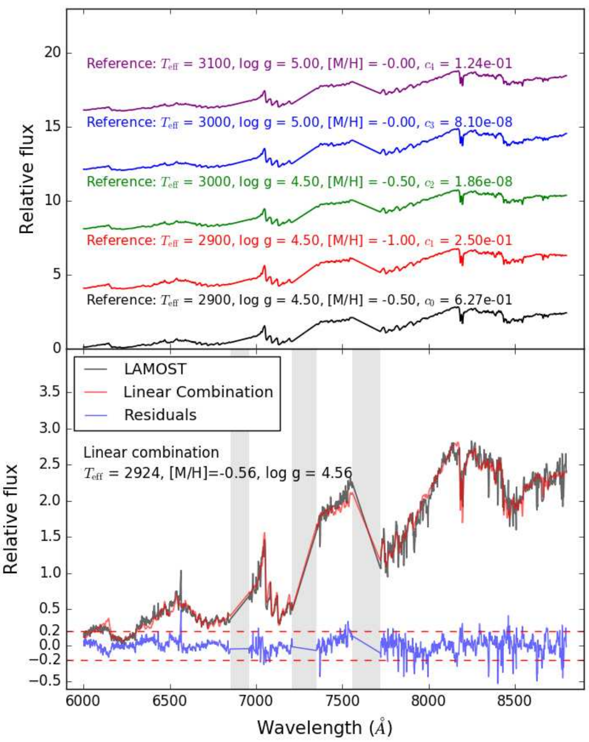


**Fig. 7** The five best-matching reference spectra used in the linear combination procedure, with their respective coefficients (*upper*). We add different constants to each of the five reference spectra for easier read. The new composite spectrum (*red*), the LAMOST target spectrum (*black*), and their residuals (*blue*) are shown in the lower panel.

part. Accordingly, we chose the spectral region of 6000 – 8800 Å including key features in it, i.e. the molecular TiO bands around 7050 and 8430 Å which are very sensitive to $T_{\rm eff}$ but almost insensitive to log *g*, and the K- and Na- line pairs at around 7680 Å and 8190 Å, which show large alterations of their line wings because of pressure broadening and are more sensitive to log *g*. In addition, the TiO bands and the alkali lines are strongly dependent on metallicity.

Effects of lines from the Earth's atmosphere have to be considered when chose the spectral regions, which should be masked during the fitting. There are four regions: 6850–6960 Å, 7210–7350 Å, 7560–7720 Å, and 8105–8240 Å contaminated by the atmospheric lines. The contamination of Na-line is weaker than that of K-line. To test whether the mask of Na-line affects the measurements of parameters, we performed internal cross-validations using the BT-Settl synthetic spectra of different masks, including no mask, mask (6850–6960 Å, 7210–7350 Å, 7560–7720 Å), and mask (6850–6960 Å, 7210–7350 Å, 7560–7720 Å, 8105–8240 Å). Each spectrum in the library can be treated as an unknown target and its parameters were calculated from the remaining library spectra. Then the derived parameters are compared with their actual parameters. The differences between actual parameters and the derived parameters of different masks are shown in Figure 3. We found that the estimated atmospheric parameters with the reserved Na-line region are comparable to the results of no mask. Therefore, we excluded 6850–6960Å, 7210–7350Å, and 7560–7720 Å from the fit procedure. Figure 4 shows an example of five stars, and indicates the masked regions in the gray filled blocks.

### 3.3 Spectral Pre-processing

Two pre-processing steps in the pipeline are needed before calculating the $\chi^2$ matching, one is the determination of the spectroscopic RV to shift the observed spectra back to the rest frames, and the other is the correction of flux which reduces the fitting residuals.

#### *3.3.1 The adopted radial velocities*

Since TiO, VO and metal hydrides dominate the optical spectral energy distribution (SED) of M-type stars, it is very challenging to determine their accurate RVs because of these complex and crowded bands. In addition to the RV from LAMOST 1D pipeline, we estimated another RV from a cross-correlation procedure. RV of LAMOST 1D pipeline were computed through $\chi^2$ between the observed spectra and templates constructed from the LAMOST spectra, while the other one is estimated from a cross-correlation procedure using the BT-Settl templates. In the cross-correlation procedure, we adopted a fifth order multiplicative polynomial to absorb the differences between the LAMOST spectra and the BT-Settl temples. To obtain a better RV, we compared the two RVs, and we chose the one with the smaller absolute value considering that large RVs are generally unreliable. Figure 5 showed the differences between the two RVs, and we can see that the two RVs are fairly consistent for most stars. It should be noted that the stellar parameter errors introduced by RV error are limited at R $\sim$ 1800 if the latter are not up to 100 $\rm km\,s^{-1}$.

#### *3.3.2 Flux error correction*

The details of flux calibration for LAMOST spectra in the official pipeline can be found in Du et al. (2016). The LAMOST flux calibration is a relative one that the uncertainty of the continuum shape still exists caused by Galactic reddening. For M-type stars, it is more difficult to obtain a pseudo-continuum due to the crowded band

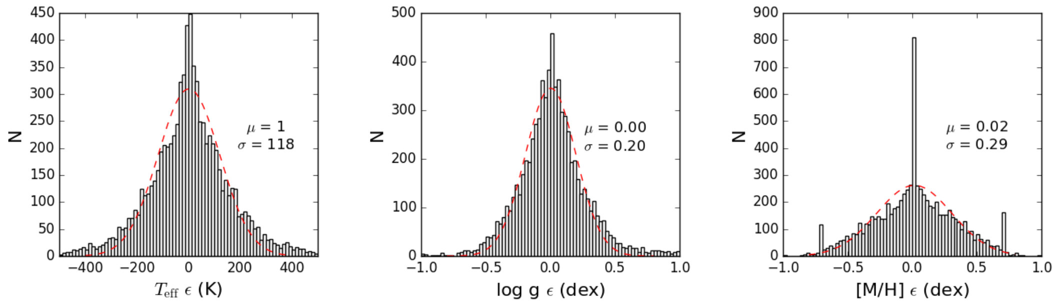


**Fig. 8** Histograms of $\epsilon$ for $T_{\rm eff}$ (*left*), log $g$ (*middle*) and [M/H] (*right*). The distribution is fitted by Gaussian shown in *red dashed curves*; The parameter offset and precision for the three parameters are labeled.

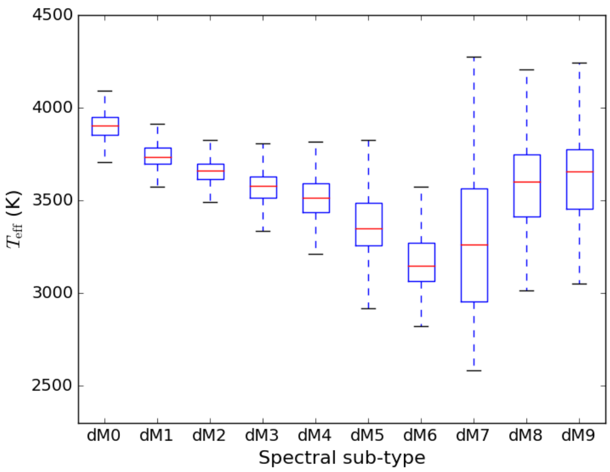


**Fig. 9** The temperature distributions of dM0 to dM9. The *box* extends from the lower to upper quartile values of the LASPM temperatures, with a *line* at the median.

structures. This makes the spectral normalization in M-type stars very challenging. The pipeline adopts a fifth order multiplicative polynomial to absorb the differences between the observed and synthetic spectra. Figure 6 shows one example of the LAMOST target spectrum (black) and one example of BT-Settl spectrum (blue). Applying a multiplicative polynomial, the adjusted BT-Settl spectrum holds the same pseudo-continuum with the target spectrum (red curve in Fig. 6). Since each template needed to be adjusted, this procedure is computationally expensive.

### 3.4 Template Matching and Linear Combination

Once the pseudo-continuum of reference spectra have been adjusted according to a target spectrum, a $\chi^2$ algorithm is used by the pipeline to compare the target spectrum with each of the adjusted reference spectra. Five best-matching reference spectra can be found through sorting $\chi^2$ . Then,

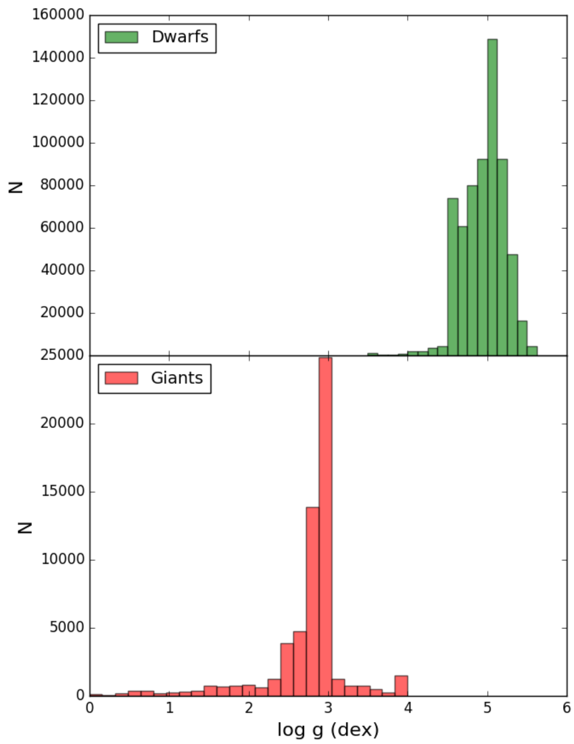


**Fig. 10** Histograms of log $g$ for dwarfs (*green*), and giants (*red*).

the parameter of this star can be interpolated among the five references by linearly combining the five best-matching spectra. A new composite spectrum is created, $S_{\rm new} = \sum_{i=1}^{5} c_i S_i$, where $S_i$ is each spectrum of the five best-matching spectra, and $c_i$ is the coefficient. We chose to use five spectra in the linear combination procedure following the work of Yee et al. (2017). A nonlinear least-squares minimization is used to find the coefficients $\{c_i \mid i = 1, 2, ..., 5\}$, minimizing $\chi^2$ when compared with

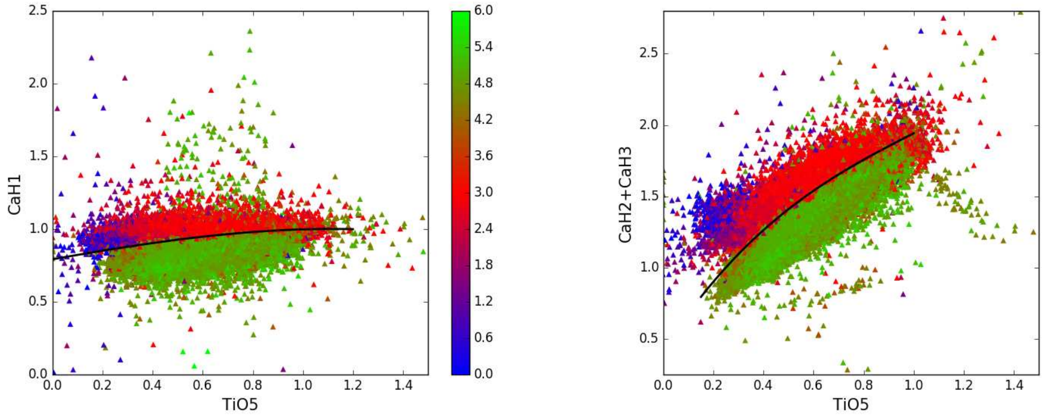


**Fig. 11** The surface gravity in the spectral indices diagrams for [CaH1, TiO5] (*left*) and [CaH2 + CaH3, TiO5] (*right*), color-coded by the log $g$ values.

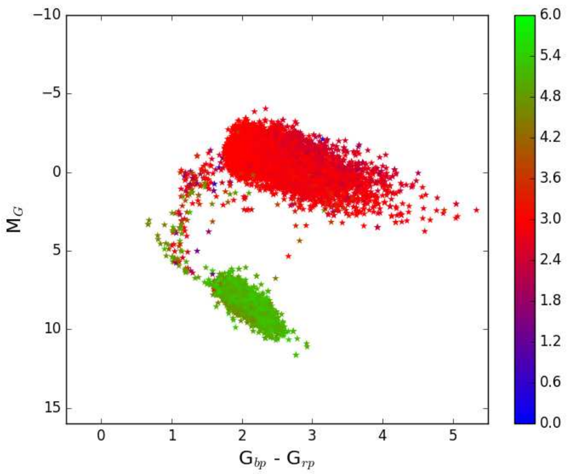


**Fig. 12** The surface gravity on Gaia color-magnitude diagram, color-coded by the log $g$ values.

the target spectrum. The $\chi^2$ was calculated through using the flux errors as weights, and the set of coefficients was constrained to that they sum to unity. Figure 7 shows an example of the linear combination for one LAMOST target. Finally, we took the weighted average of the reference parameters as the target parameters.

## 4 THE RESULTS OF LASPM

We applied LASPM to 687 916 M-type spectra in DR7. We analyzed giants and dwarfs separately, and the classifications of giants and dwarfs are inherited from the 1D pipeline. For giants, we used the grids with $0.0 \leq \log g \leq 4.0$ dex, while for dwarfs, we used the grids with $3.5 \leq \log g \leq 6.0$ dex. Ultimately, we determined stellar parameters for 680 185 out of 687 916 M-type spectra. The failure of parameter measurements for the 7731 spectra

**Table 2** Parameter Ranges of the Two Sub-grids Used by ASPCAP for M-type Stars

| | M Giant | M Dwarf |
|---|---|---|
| $T_{\rm eff}$ (K) | 3000 – 4000 (100, 11) | 3000 – 4000 (100, 11) |
| log $g$ (dex) | –0.5 – +3.5 (0.5, 8) | +2.5 – +5.5 (0.5, 7) |
| $[{\rm M/H}]$ (dex) | –2.5 – +1.0 (0.25, 15) | –2.5 – +1.0 (0.25, 15) |
| $[\alpha/{\rm Fe}]$(dex) | –0.75 – +1.0 (0.25, 8) | –0.75 – +1.0 (0.25, 8) |

was because that there were too many bad points in our chosen region.

### 4.1 Precision

We estimated the parameter precision from the parameter measurements of the multiple observations for the same stars. Since the instrinsic precisions of stellar parameters depend on spectral S/N strongly when the S/N is low, to reduce the error introduced by spectral S/N, we abandoned the observations with spectral S/N $< 10$. The precision is measured by a statistical estimator:

$$\epsilon = \sqrt{\frac{\rm N}{\rm N-1}} \times ({\rm P_i} - \overline{\rm P}) \,, \tag{1}$$

where N is the number of times for repeated observations, $\rm P_i$ is the parameters ($T_{\rm eff}$, log $g$ and [M/H]) of the $\rm i_{th}$ observation, and $\overline{\rm P}$ is $\frac{1}{\rm N}\sum_{\rm i}^{\rm N} {\rm P_i}$.

Figure 8 shows the Gaussian fits to the $\epsilon$ distributions of $T_{\rm eff}$ , log $g$ and [M/H]. The precision we achieved in terms of $1\sigma$ uncertainties of the $\epsilon$ distributions is 118 K for $T_{\rm eff}$, 0.20 dex for log $g$, and 0.29 dex for [M/H]. We found that the metallicity estimate had a larger dispersion than log $g$. This is partly because of the sparse metallicity grid with a step of 0.5 dex. In addition, the spatial distribution of metallicity grid is not uniform with 38.4% of [M/H] = +0.0 dex and 35.3% of [M/H] $<$ –0.5. This allows the metallicities of Sun-like abundance stars to be probably linear interpolated to the grid point of [M/H] = +0.0 dex,

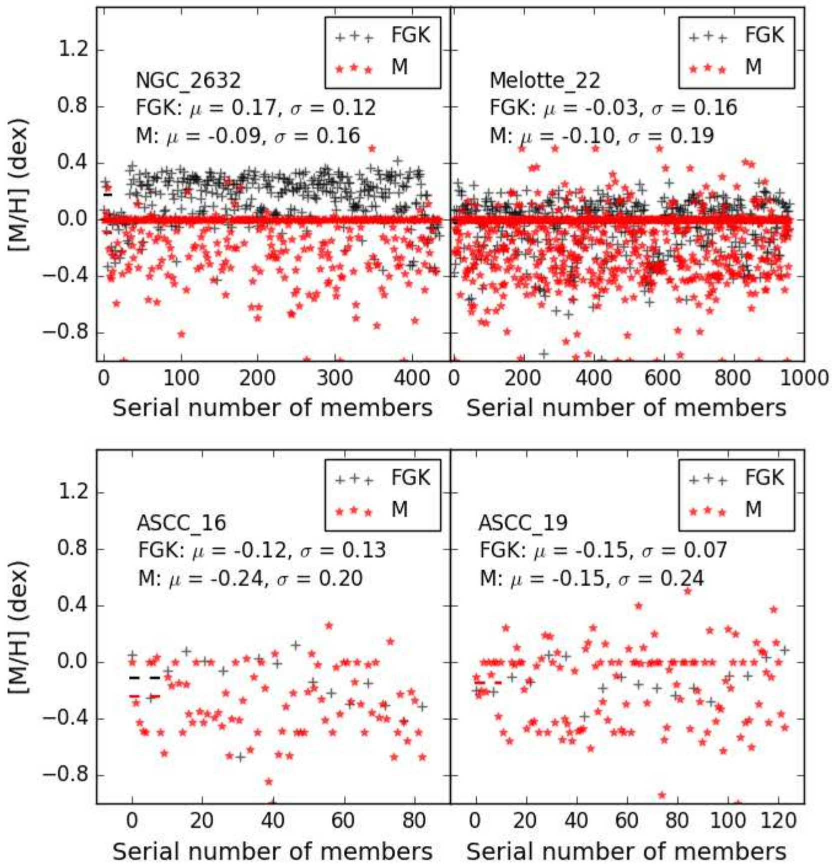


**Fig. 13** Distributions of metallicity for the members of four open clusters. The mean and dispersion of metallicity for each cluster are also marked.

because the five best matches are all of [M/H] = +0.0 dex. Another small sample clusters at [M/H] $\sim$ –1.0 dex due to the sharp fall of numbers of metal-poor templates. For metal-poor stars, the five best-matched template spectra have large differential gradients. This makes the linear combination coefficients having one coefficient close to 1.0 and others close to 0.0. As a result, the interpolated metallicity approaches the grid point of [M/H] = –1.0. The two samples with the bigger one at [M/H] = +0.0 dex and the smaller one at [M/H] $\sim$ –1.0 dex resulted in the three peaks in the right panel of Figure 8. Moreover, the metallicity of M-type stars is much difficult to obtain than temperature and surface gravity. Other than earlier type stars, the dense forest of spectral features in M-type stars is more challenging. As a result, contradicting metallicities have been giving in literatures for decades.

### 4.2 Effective Temperature, $T_{\rm eff}$

To evaluate our temperature results, we presented the temperature distributions of dM0 to dM9. Considering the influence of the other two parameters on spectral classification, we selected stars by limiting log $g$ and [M/H] in the range from 4.0 to 5.5 dex and from –0.5 to +0.5 dex, respectively. The temperature distributions of dM0 to dM9 were shown in Figure 9. From dM0 to dM6, our results for temperature were consistent with the spectral classifications of 1D pipeline. However, the temperature was overestimated for stars cooler than dM6. At cooler temperatures, TiO bands start to saturate (Passegger et al. 2016). For giants, we did not show their temperature distributions due to the limited number of stars.

### 4.3 Surface Gravity, log *g*

From Figure 10, we note that surface gravities of LASPM are consistent with the luminosity classes by 1D pipeline, with peaks at 2.9 dex for giants and 5.0 dex for dwarfs. To verify the surface gravities, we calculated a set of four spectral band indices in LAMOST spectra: CaH1, CaH2, CaH3, and TiO5 defined in the work by Zhang et al. (2019)

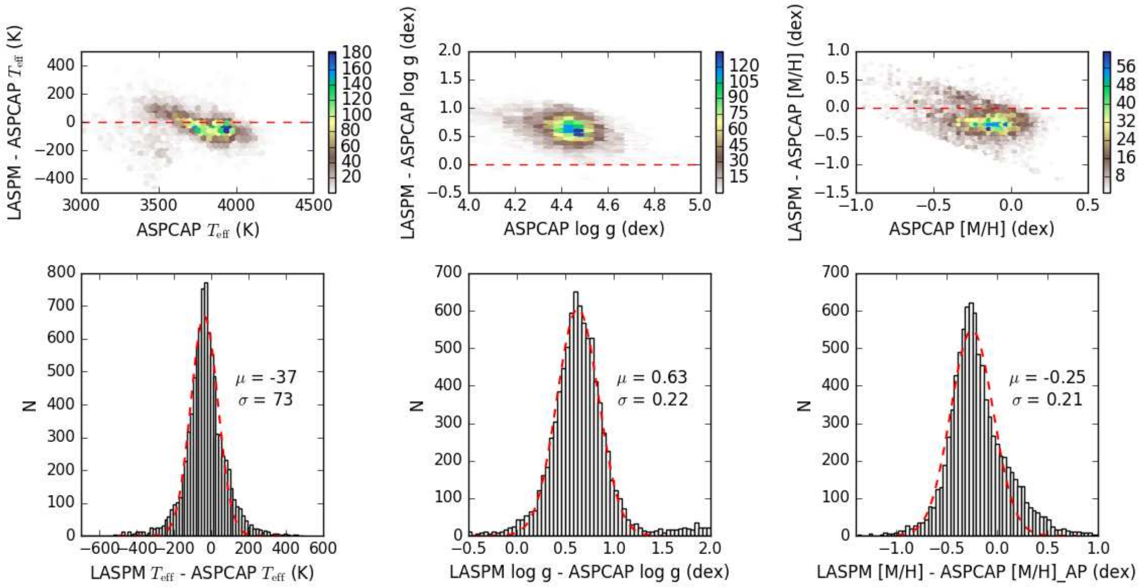

**Fig. 14** Comparison of stellar parameters between by LASPM and by ASPCAP. Upper panel: contour distributions of differences between the ASPCAP parameters and LASPM parameters. Lower panel: histograms of differences between our results and the ASPCAP stellar parameters, and they are fitted using Gaussian shown as *red dashed curves*. The mean and dispersion of the Gaussian are also labeled.

as surface gravity indicators. Figure 11 superimposes the log $g$ values of stars on their spectral index [CaH1, TiO5] and [CaH2 + CaH3, TiO5] diagrams by color. We can see clear separators on both [CaH1, TiO5] and [CaH2 + CaH3, TiO5] diagrams to differentiate between gM and dM, which indicates that our log $g$ results agree with the locations on the spectral indice diagrams.

To further verify surface gravity of LASPM, we exhibited common stars' locations on $G$ absolute magnitude versus BP - RP diagram by cross-matching the LAMOST M-type stellar parameter catalog with Gaia Data Release 2 (DR2). After exclusion of the stars having a large parallax error (parallax_error/parallax $>$ 0.2), there were 25 076 stars in both catalogs. We abandoned the spectra tagged 'Unknown' by manual inspection, and obtained 24 853 common stars. Figure 12 shows their locations on Gaia color-magnitude diagram. Although the observed colors are not corrected for reddening, the giant and dwarf loci are obvious on the color-magnitude diagram, which means the surface gravity results obtained by the LASPM are consistent with their locations on color-magnitude diagram. We inspected the 17 spectra with Gaia BP-RP $<$ 1.0 and found that they are probably late K-type stars but recognized as early M. We noted the tail of red clump around M_G $\sim$ 0.0 and BP-RP $\sim$ 1.5. The red clump has a long tail in the color-absolute magnitude diagram due to interstellar extinction (Gaia Collaboration et al. 2019).

### 4.4 Metallicity, [M/H]

It is difficult to determine accurate metallicity in M-type stars due to the dense forest of spectral features. For low-mass stars, the spectral energy distribution (SED) can be severely affected by metallicity, which is different to Sun-like stars. Accordingly, the SED uncertainties in M-type stars associated with data reduction lead to a larger error in the metallicity determination, when compared to Sun-like stars. This would explain why the metallicity of M-type stars has a poor precision.

To validate our results for metallicity, we analyzed the metallicity estimates for selected members of four open clusters (NGC 2632, Melotte 22, ASCC_16 and ASCC_19). As a reference set for comparison, the metallicity of FGK-type members of the four open clusters were also analyzed. The metallicity distributions of members are shown in Figure 13. The LASP results of metallicity have been validated, having a precison of $\sim$ 0.1 dex (Luo et al. 2015; Du et al. 2019). No obvious systematic offset is found for the metallicity of FGK-type stars when compared to other catalogs except for low-metallicity stars (Du et al. 2019). Our results for metallicity in M-type stars agree with the results in FGK-type stars belonging to the same cluster, except that the former has a little larger dispersion and a non-Gaussion distribution due to the non-uniform metallicity distribution of BT-Settl grid. Both results of M- and

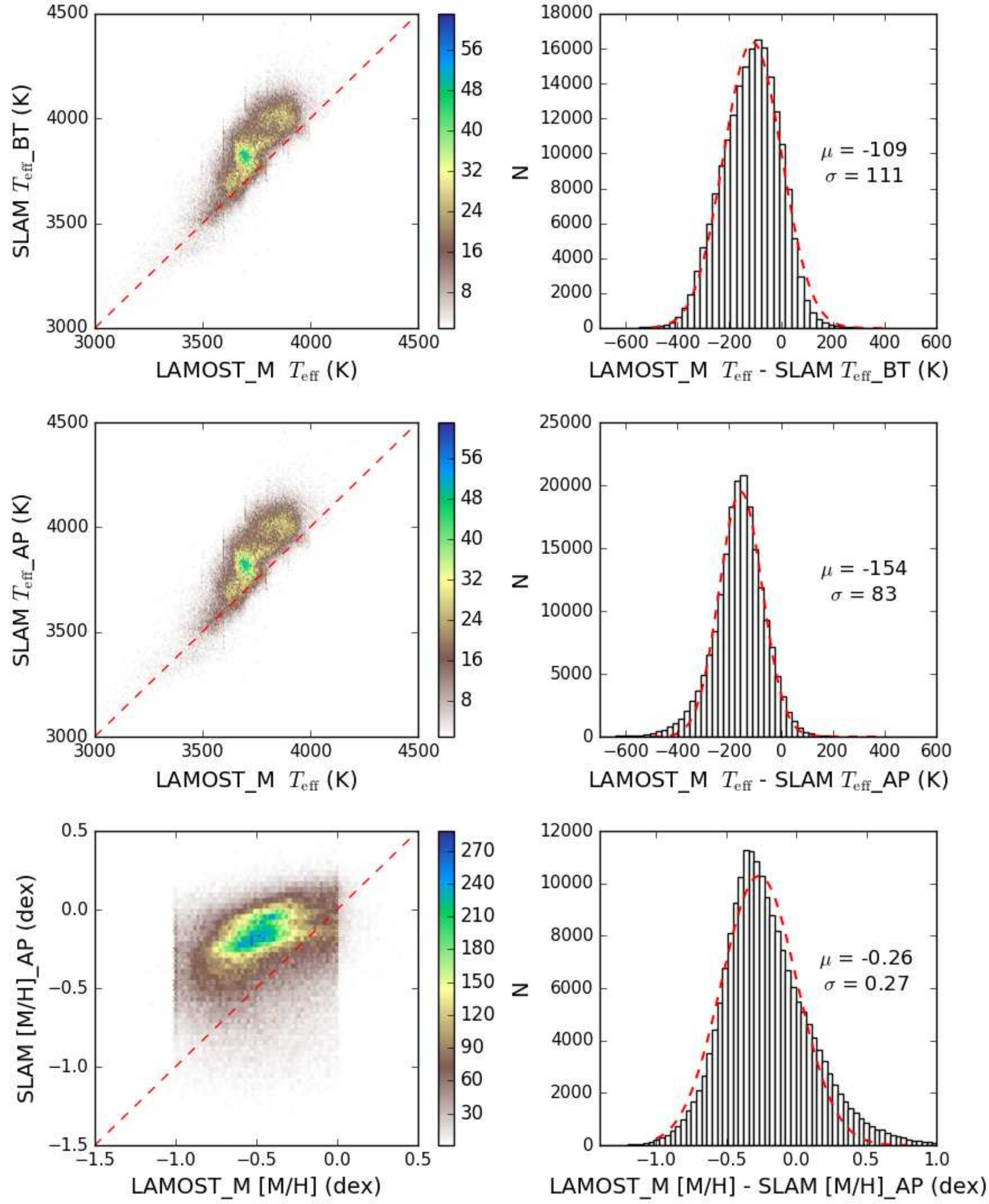


**Fig. 15** Comparison of stellar parameters between by LASPM and by SLAM. The *diagonal dashed lines* shown in the left column represent one-to-one correspondence. *Histograms* shown in the right column are differences between our results and the SLAM stellar parameters, and they are fitted using Gaussian shown as *red dashed curves*. The mean and dispersion of the Gaussian are also labeled.

FGK-type members are consistent with the metallicity of open clusters (Netopil et al. 2016). We find no obvious systematic offset in our results for metallicity.

### 4.5 Comparison with APOGEE

The measurement of stellar parameters in M-type stars was performed by the APOGEE Stellar Parameter and Chemical Abundance Pipeline (ASPCAP; García Pérez et al. 2016) from the high-resolution near infrared spectra. The APOGEE of the SDSS DR16 included about 473 307 spectra of 437 445 stars, for which the parameters were updated using the latest version of pipelines (Jönsson et al. 2020). The ASPCAP measured stellar parameters of M-type stars by using a grid of cooler Model Atmospheres in Radiative and Convective Scheme (MARCS) models (Gustafsson et al. 2008). The parameter ranges used by ASPCAP for M-type stars were presented in Table 2. We cross-matched the LAMOST M-type stellar parameter catalog with the APOGEE DR16 and obtained 17 845 spectra of 10 392 common stars. We abandoned the spectra with LAMOST $S/N_i < 10$ and excluded the ones with the parameters that the pipeline gives at the boundary grid values. Finally, a total of 8925 spectra including repeated observations were left.

We compared our results with the ASPCAP spectroscopic stellar parameters, which achieved the best fit between the synthetic and observed spectrum. Figure 14 shows the comparison of the two catalogs. The differences between our results and the ASPCAP spectroscopic stellar parameters have a scatter of 73 K in $T_{\rm eff}$, 0.22 dex in log *g*, and 0.21 dex in [M/H]. We note that our results for surface gravity are overestimated by about 0.63 dex. This may be related to different reference templates and different spectral regions. As for metallicity, Our results are underestimated by about 0.25 dex.

### 4.6 Comparison with SLAM

Li et al. (2020) determined $T_{\rm eff}$ and [M/H] for about 300 000 M dwarf stars observed by both LAMOST and Gaia using Stellar Label Machine (SLAM). They trained two SLAM models, one model used LAMOST spectra with APOGEE DR16 labels and the other was trained by the BT-Settl atmospheric model. $T_{\rm eff}$_BT was the temperature through the SLAM model trained by BT-Settl while $T_{\rm eff}$_AP and [M/H]_AP were determined by the SLAM model with APOGEE labels. The comparison between our results and the SLAM paramters was shown in Figure 15. The LASPM $T_{\rm eff}$ is consistent with $T_{\rm eff}$_BT and $T_{\rm eff}$_AP with a scatter of 111 K and 83 K, respectively. However, there is a systematic offset between the LASPM $T_{\rm eff}$ and the SLAM $T_{\rm eff}$. The SLAM overestimated the temperature by about 100 K. The differences between LASPM [M/H] and [M/H]_AP have a scatter of 0.27 dex and a offset of 0.26 dex, which is consistent with the differences between the LASPM [M/H] and the APOGEE [M/H]. We noted a small sample clustered at [M/H] $\sim$ -1.0 due to the sharp fall of numbers of metal-poor templates. A denser and more uniform grid is needed to achieve better metallicity results.

## 5 SUMMARY AND DISCUSSION

We developed the so called LASPM pipeline to determine the atmospheric parameters from LAMOST low-resolution optical spectroscopy in M-type stars with the updated BT-Settl model grids. The parameters are determined by comparing the observed spectra to synthetic spectra, minimizing $\chi^2$ through a linear combination of five best-matching templates. The pipeline is applied to 680 185 M-type spectra for LAMOST DR7 (including 610 419 released in DR6), and two atmospheric parameter catalogs of M-type stars are formally released in DR6 and DR7, respectively. The LASPM extends the LASP parameters to cool stars.

We estimated the intrinsic precision of the parameter measurements using the repeat observations for the same stars. The precision is 118 K for $T_{\rm eff}$, 0.20 dex for log *g*, and 0.29 dex for [M/H]. From dM0 to dM6 with solar abundance, our results for $T_{\rm eff}$ are consistent with the spectral classifications of 1D pipeline. Our results for surface gravity are consistent with the luminosity classes by 1D pipeline, and also agree with their locations both on the spectral indices and color-magnitude diagrams. We analyzed the metallicity estimates for selected members of four open clusters (NGC 2632, Melotte 22, ASCC_16 and ASCC_19). Our results for metallicity are consistent with the metallicity of open clusters without a systematic offset. We compared our results with the ASPCAP spectroscopic stellar parameters. The scatter of differences are 73 K, 0.22 dex, 0.21 dex in $T_{\rm eff}$, log *g*, and in [M/H], respectively. Except for a systematic offset, our results are basically consistent with those of SLAM (Li et al. 2020) with a scatter of $\sim$ 100 K in $T_{\rm eff}$ and 0.27 dex in [M/H].

The pipeline overestimates the temperature in stars cooler than dM6, which might be caused by the saturation of TiO bands at cool temperature (Passegger et al. 2016). For M dwarfs, the surface gravities are overestimated by the pipeline in about 0.63 dex when compared to the ASPCAP; while for giants, the surface gravities are overestimated more. This might be related to different parameter coverages of different model grids. The metallicities are underestimated by the pipeline in about 0.25 dex against the ASPCAP metallicity. Metallicity of M-type stars is more difficult to estimate than temperature and surface gravity, which is more related to the SED, and it is a challenge to locate its SED due to the dense forest of spectral features in M-type stars. Accordingly, the SED uncertainties in M-type stars associated with data reduction lead to a larger error in the metallicity, when compared to Sun-like stars.

**Acknowledgements** This work is supported by is supported by the National Natural Science Foundation of China (Grant Nos. U1931209 and 12090044) and the National Key R&D Program of China (Nos. 2019YFA0405502 and 2019YFA0405102).

Guo Shou Jing Telescope (the Large Sky Area Multi-Object Fiber Spectroscopic Telescope, LAMOST) is a National Major Scientific Project built by the Chinese Academy of Sciences. Funding for the project has been provided by the National Development and Reform Commission. LAMOST is operated and managed by the

National Astronomical Observatories, Chinese Academy of Sciences.

## References

Allard, F., Hauschildt, P. H., Alexander, D. R., et al. 2001, ApJ, 556, 357
Allard, F., Homeier, D., & Freytag, B. 2011, 16th Cambridge Workshop on Cool Stars, Stellar Systems, and the Sun, 448, 91
Allard, F., Homeier, D., Freytag, B., et al. 2012, EAS Publications Series, 57, 3
Allard, F., Homeier, D., Freytag, B., et al. 2013, Memorie Della Societa Astronomica Italiana Supplementi, 24, 128
Barber, R. J., Tennyson, J., Harris, G. J., et al. 2006, MNRAS, 368, 1087
Boyajian, T. S., von Braun, K., van Belle, G., et al. 2012, ApJ, 757, 112
Caffau, E., Maiorca, E., Bonifacio, P., et al. 2009, A&A, 498, 877
Caffau, E., Ludwig, H.-G., Steffen, M., et al. 2011, Sol. Phys., 268, 255
Chowdhury, P. K., Merer, A. J., Rixon, S. J., et al. 2006, Physical Chemistry Chemical Physics (Incorporating Faraday Transactions), 8, 822
Cui, X.-Q., Zhao, Y.-H., Chu, Y.-Q., et al. 2012, RAA (Research in Astronomy and Astrophysics), 12, 1197
Deng, L.-C., Newberg, H. J., Liu, C., et al. 2012, RAA (Research in Astronomy and Astrophysics), 12, 735
Du, B., Luo, A.-L., Kong, X., et al. 2016, ApJS, 227, 27
Du, B., Luo, A.-L., Zuo, F., et al. 2019, ApJS, 240, 10
Dulick, M., Bauschlicher, C. W., Burrows, A., et al. 2003, ApJ, 594, 651
Gaia Collaboration, Eyer, L., Rimoldini, L., et al. 2019, A&A, 623, A110
García Pérez, A. E., Allende Prieto, C., Holtzman, J. A., et al. 2016, AJ, 151, 144
Gustafsson, B., Edvardsson, B., Eriksson, K., et al. 2008, A&A, 486, 951
Jönsson, H., Holtzman, J. A., Allende Prieto, C., et al. 2020, AJ, 160, 120
Li, J., Liu, C., Zhang, B., et al. 2020, arXiv:2012.14080
Luo, A.-L., Zhao, Y.-H., Zhao, G., et al. 2015, RAA (Research in Astronomy and Astrophysics), 15, 1095
Netopil, M., Paunzen, E., Heiter, U., et al. 2016, A&A, 585, A150
Passegger, V. M., Wende-von Berg, S., & Reiners, A. 2016, A&A, 587, A19
Plez, B. 1998, A&A, 337, 495
Rajpurohit, A. S., Reylé, C., Allard, F., et al. 2013, A&A, 556, A15
Rajpurohit, A. S., Reylé, C., Allard, F., et al. 2016, A&A, 596, A33
Rajpurohit, A. S., Allard, F., Rajpurohit, S., et al. 2018, A&A, 620, A180
Rojas-Ayala, B., Covey, K. R., Muirhead, P. S., et al. 2012, ApJ, 748, 93
Ségransan, D., Kervella, P., Forveille, T., et al. 2003, A&A, 397, L5
Skory, S., Weck, P. F., Stancil, P. C., et al. 2003, ApJS, 148, 599
Weck, P. F., Schweitzer, A., Stancil, P. C., et al. 2003, ApJ, 584, 459
Yee, S. W., Petigura, E. A., & von Braun, K. 2017, ApJ, 836, 77
York, D. G., Adelman, J., Anderson, J. E., et al. 2000, AJ, 120, 1579
Yurchenko, S. N., Barber, R. J., & Tennyson, J. 2011, MNRAS, 413, 1828
Zhang, S., Luo, A.-L., Comte, G., et al. 2019, ApJS, 240, 31